Editors' Suggestion

Engineering the Impact of Phonon Dephasing on the Coherence of a WSe_2 Single-Photon Source via Cavity Quantum Electrodynamics

Victor N. Mitryakhin,[1,*] Alexander Steinhoff,[2] Jens-Christian Drawer,[1] Hangyong Shan,[1] Matthias Florian,[3] Lukas Lackner,[1] Bo Han,[1] Falk Eilenberger,[4] Seth Ariel Tongay,[5] Kenji Watanabe,[6] Takashi Taniguchi,[7] Carlos Antón-Solanas,[8] Ana Predojević,[1,9] Christopher Gies,[2] Martin Esmann,[1] and Christian Schneider[1]

[1]*Carl von Ossietzky Universität Oldenburg, Fakultät V, Institut für Physik, 26129 Oldenburg, Germany*
[2]*Institute for Theoretical Physics and Bremen Center for Computational Material Science, University of Bremen, 28334 Bremen, Germany*
[3]*University of Michigan, Department of Electrical Engineering and Computer Science, Ann Arbor, Michigan 48109, USA*
[4]*Friedrich Schiller University Jena, Jena, Germany*
[5]*Materials Science and Engineering, School for Engineering of Matter, Transport and Energy, Arizona State University, Tempe, Arizona 85287, USA*
[6]*Research Center for Functional Materials, National Institute for Materials Science, 1-1 Namiki, Tsukuba 305-0044, Japan*
[7]*International Center for Materials Nanoarchitectonics, National Institute for Materials Science, 1-1 Namiki, Tsukuba 305-0044, Japan*
[8]*Depto. de Física de Materiales, Instituto Nicolás Cabrera, Instituto de Física de la Materia Condensada, Universidad Autónoma de Madrid, 28049 Madrid, Spain*
[9]*Department of Physics, Stockholm University, 10691 Stockholm, Sweden*

(Received 20 July 2023; revised 26 February 2024; accepted 22 March 2024; published 16 May 2024)

Emitter dephasing is one of the key issues in the performance of solid-state single-photon sources. Among the various sources of dephasing, acoustic phonons play a central role in adding decoherence to the single-photon emission. Here, we demonstrate that it is possible to tune and engineer the coherence of photons emitted from a single WSe_2 monolayer quantum dot via selectively coupling it to a spectral cavity resonance. We utilize an open cavity to demonstrate spectral enhancement, leveling, and suppression of the highly asymmetric phonon sideband, finding excellent agreement with a microscopic description of the exciton-phonon dephasing in a truly two-dimensional system. Moreover, the impact of cavity tuning on the dephasing is directly assessed via optical interferometry, which points out the capability to utilize light-matter coupling to steer and design dephasing and coherence of quantum emitters in atomically thin crystals.

DOI: 10.1103/PhysRevLett.132.206903

In contrast to excitations in isolated atoms, an appropriate understanding of the light-matter coupling of excitons in solid-state quantum emitters cannot be developed without considering the crucial impact of the lattice environment. In the context of emission of quantum light, it is the coupling of excitons to acoustic phonons in most semiconductors that manifests itself via the formation of spectral sidebands and replica modes [1–3].

While such phenomena can be directly employed in quantum-optomechanic experiments [4–10], they typically impede the coherence of the emitted light in material-specific manners. Atomically thin crystals belong to the most intriguing class of quantum materials utilized in modern photonic research [11]. Because of their ultimate thinness, the correlations of carriers are strongly enhanced and dominate their optical response. In the presence of random or engineered local strain, the formation of luminescent hot spots has been verified [12,13], displaying nonclassical light emission. Such quantum dots (QDs) can be found in the majority of thin-layer transition metal dichalcogenide (TMDC) crystals. However, they are particularly pronounced in WSe_2 mono- and bilayers, which have been extensively studied in this regard [12,14–17]. QDs in TMDCs have recently shifted into the spotlight of quantum photonic research. In contrast to conventional quantum emitters in bulk material, two-dimensional QDs are highly tunable without the need for demanding semiconductor processing [15,18]. They can be conveniently integrated into photonic architectures without the restrictions of lattice matching [19], which can be realized via simple low-cost pick-and-place methods [20].

Despite this ease of integrating TMDC QDs into photonic devices, the enhancement of spontaneous emission from monolayer QDs has been demonstrated in a limited number of reports. The Purcell regime has been verified using TMDC Bragg gratings [21], plasmonic structures [22–24], and most recently in tunable open optical cavities [25].

While it is clear that dephasing channels compromise and dictate the coherence of the emitted photons, they are yet to be exhaustively studied. It is possible to engineer crystal superlattices on the nanoscale to suppress coupling to phonons in specific frequency bands, however, such approaches are typically technologically too demanding to be routinely implemented with single quantum emitters [26–31]. Up to now, spectral wandering has been identified as one of the main sources of decoherence in the emission of 2D crystal QDs [32–34]. In addition, it was shown that due to the large Huang-Rhys factor of WSe_2, the coupling to phonons is extraordinarily strong and induces a very rich phonon-sideband spectrum [35].

Here, we demonstrate that the unique shape of the phonon sideband in WSe_2 QDs can be exploited to engineer its coherence properties via emitter-cavity coupling. Specifically, by tuning the optical resonance of our cavity system to match either the zero-phonon emission line (ZPL) or the phonon sideband (PSB), we control the individual contributions of these two features to the overall emission spectrum. As a result, the temporal coherence of the single-photon emission can be manipulated, changing from a slowly decaying single exponential trace to a biexponential trace as the cavity resonance is tuned across the emission spectrum.

The WSe_2 monolayer is placed on the surface of a mirror that is part of an asymmetric plano-concave open cavity [depicted in Fig. 1(a)]. The cavity consists of two mirrors that are freely movable. The monolayer hosts QDs arising from crystalline defects. The emission from one of the QDs is investigated. The QD is driven by a pulsed Ti:sapphire laser operating at a central energy of 1.722 eV. Further details of the cavity system can be accessed in Supplemental Material [36].

Prior to the studies of photoluminescence (PL) from the QD inside the cavity, the QD emission without a cavity is investigated [see Fig. 1(b)]. A PL spectrum of the QD features a pronounced ZPL and a lower-energy PSB. Figure 1(b) shows the ZPL spectrum located at approximately 1.596 eV, with a linewidth of 110 ± 3 μeV (spectrometer resolution limited). The linewidth of the PSB is 0.7 ± 0.1 meV. The ZPL and PSB are separated by 0.6 meV resulting in an asymmetric shape of the emission spectrum [see the inset of Fig. 1(b) plotted in logarithmic scale].

To verify the quantum character of the PL emission, we implement a second-order correlation measurement [see Fig. 1(c)] resulting in $g^2(0) = 0.105 \pm 0.007$. The measurement is carried out in a resonant cavity-QD configuration profiting from the significant signal enhancement.

The resonant enhancement of photon flux is a direct consequence of the modification of the emitter decay rate and light distribution in the cavity via the Purcell effect [49]. The modification of the luminescence while sweeping the cavity resonance through the QD ZPL is shown in Fig. 1(d). These PL spectra are plotted vs the cavity-emitter detuning $\delta = \hbar\omega_{\mathrm{cav}} - \hbar\omega_0$, where $\hbar\omega_{\mathrm{cav}}$ is the energy of the cavity resonance and $\hbar\omega_0$ is the ZPL energy [at 1.596 eV; see Fig. 1(d), and extracted PL spectra for several detunings in Fig. 2(a)]. When the ZPL is in resonance with the cavity, the intensity of the emission is enhanced by more than a factor of 6 compared to the

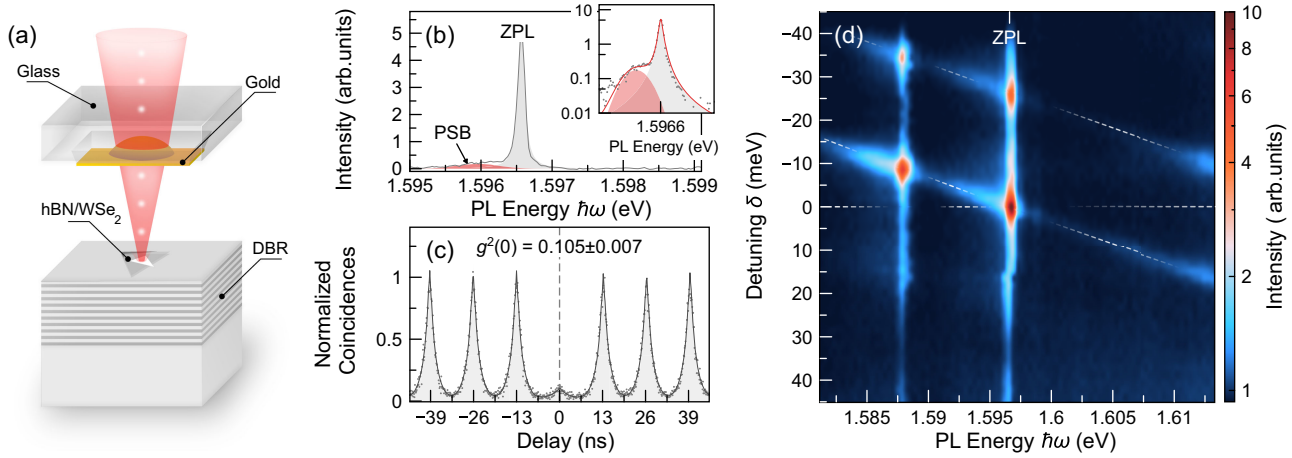

FIG. 1. (a) Schematics of the open cavity device under optical excitation. A beam is focused through the top concave mirror onto the monolayer and exciting the QD, thus triggering the emission of single photons. The generated single photons escape the cavity through the top mirror. (b) Low-resolution PL spectrum of the QD at 3.2 K recorded without the cavity top mirror. (c) Second-order correlation function. The separation of the peaks is inversely proportional to the laser repetition rate. The peaks have been fitted with an ensemble of double exponential functions $Ae^{-|x-x_0|/t}$. (d) PL spectra as a function of relative detuning of a cavity resonance from the emission energy at approximately 1.596 eV (labeled ZPL). The intensity (color coded) is plotted in $\log_{10}$ scale. The inclined dashed white lines indicate the cavity modes. As a cavity mode sweeps through emission energies, the emission is gradually enhanced making both the ZPL and PSB (the tail to the left of the ZPL) more pronounced.

off-resonant case. The PSB is affected by the cavity tuning: When the cavity is positively detuned, the contribution of the PSB to the PL spectrum is almost negligible and the ZPL dominates. For negative detunings, the PSB contribution is notable and manifests itself as a distinct spectral feature in Fig. 1(d). We study this phenomenon to quantify the interplay between the ZPL and PSB integral intensities for cavity-emission tuning by applying a fitting procedure based on the independent boson model for quantum emitters interacting with phonons in the two-dimensional monolayer [37]. We include coupling of the local emitter to two-dimensional longitudinal acoustic phonons [38] and a localized phonon mode [39]. The optical susceptibility of the QD-phonon system is

$$\chi(t) = i\theta(t)e^{-i\omega_0 t+\Phi(t)-\Gamma_{\mathrm{inhom}}^2 t^2}, \tag{1}$$

with Γ_{inhom} being the inhomogeneous broadening and $\Phi(t)$ being the phonon dephasing integral:

$$\Phi(t) = \sum_j \int_0^\infty d\omega \frac{J_j(\omega)}{\pi\omega^2}\left\{\coth\left(\frac{\hbar\omega}{2k_BT}\right)[\cos(\omega t)-1] - i\sin(\omega t)\right\}. \tag{2}$$

Here, $J_j(\omega)$ is the spectral density of phonon branch j as detailed in the Supplemental Material [36]. The corresponding emission spectrum is obtained by inverting the absorption spectrum at the ZPL:

$$I_{\mathrm{QD\text{-}PSB}}(\omega) = \alpha(2\omega_0-\omega) = \mathrm{Im}\left\{\int_{-\infty}^{\infty} dt\chi(t)e^{i(2\omega_0-\omega)t}\right\}. \tag{3}$$

The cavity is explicitly accounted for by multiplying the QD-sideband emission spectrum with a line shape function $L(\omega)$ describing the photonic density of states as discussed in the Supplemental Material [36]. Translating the modeled emission spectra to experimentally observed intensities requires an additional scaling factor a:

$$I(\omega) = a(I_{\mathrm{QD\text{-}PSB}}(\omega)+I_{\mathrm{BG}})L(\omega). \tag{4}$$

Here, background I_{BG} is added accounting for a possible contribution of a low-energy tail of another emitter and emission of the free exciton.

We simultaneously fit the datasets for several detunings with the same emitter-phonon coupling parameters. To account for experimentally determined fluctuations, only small variations of the ZPL position, the cavity parameters, and the scaling factor a are allowed with detuning. The obtained fit parameters are collected in the Supplemental Material [36]. The resulting spectral fittings are shown in Fig. 2(a). For the lowest detuning (top panel), the cavity

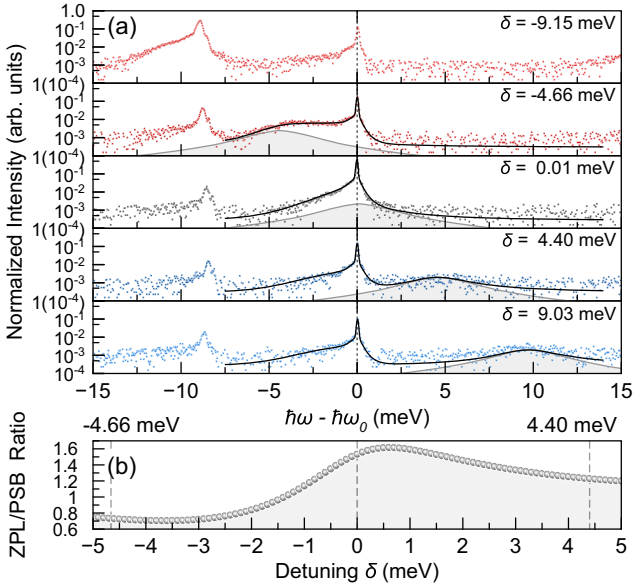

FIG. 2. (a) PL spectra (y axis is in $\log_{10}$ scale) for selected cavity-emitter detunings [−9.15, −4.66, 0.01, 4.40, 9.03] meV excited by the Ti:sapphire laser in continuous wave regime at 720 nm wavelength. The position of the cavity is indicated by the gray shaded region. The solid black lines arise from the theoretical model. From the fit, we obtain a lattice temperature of 4.6 K. (b) Ratio between the intensities of the ZPL and the PSB emission as a function of the cavity-ZPL detuning.

spectrally overlaps with the second QD (located at 1.588 eV), which hinders fitting the spectrum. As detailed in the Supplemental Material [36], our model can be analytically solved yielding a decomposition of the spectrum into phonon-assisted processes of arbitrary order. This allows us to quantify the ZPL and PSB contribution to the emission. Because of the two-dimensional nature of acoustic phonons, the carrier-phonon coupling efficiency does not vanish at small momenta, as it is the case in three dimensions [40]. Hence, the ZPL spectrally overlaps with low-energy higher-order processes that involve the absorption and emission of phonons. We sum up the zero-phonon contributions and the higher-order contributions with energies smaller than the full width at half maximum of the inhomogeneous emitter broadening to obtain an effective ZPL. A weighting of ZPL and PSB with the cavity line shape at different detunings quantifies the ZPL and PSB interplay [see Fig. 2(b)]: The resulting extracted ratio of the ZPL to the PSB is approximately 1.6 for the positively detuned cavity, indicating a regime that is dominated by the ZPL. For the negatively detuned case, it approaches 0.7, suggesting a tremendous impact of the PSB on the coherence of single photons emitted from the QD-cavity device under such detuning conditions.

To account for the limitations of conventional spectroscopy and to directly verify the impact of these phenomena on photon coherence, we extend our study with interferometric measurements in the time domain. Here, we filtered

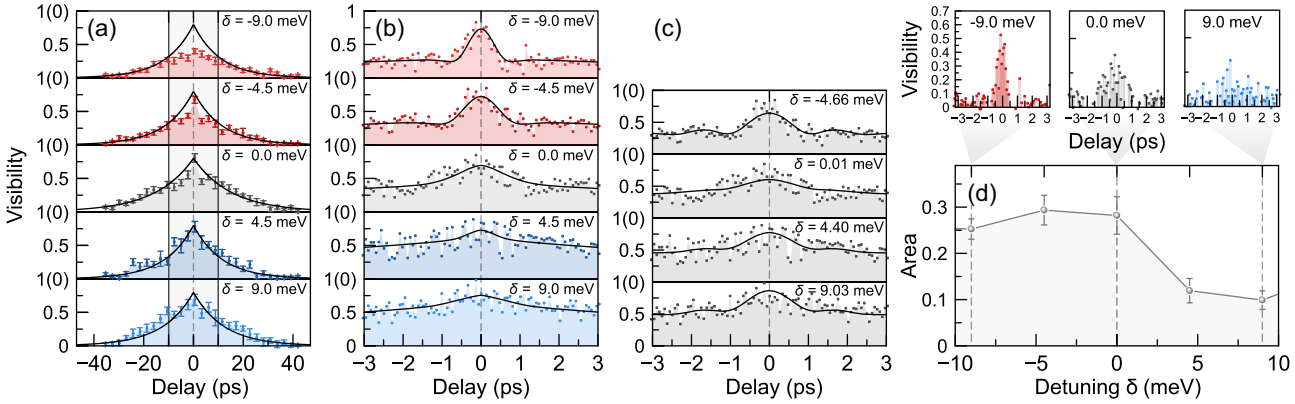

FIG. 3. Interference visibility: (a) for a large range and (b) for a small range of the time delay between the arms of the interferometer. Markers indicate the data obtained in the experiment; solid lines indicate fit functions. In panel (a), the fit is based on the tails outside of the shaded area; see explanation in the text. (c) Solid lines represent the visibility calculated as the modulus of the Fourier transformed fit functions from Fig. 2(a) including a bandpass filter model. The data are normalized to match the observed visibility of the experiment. (d) Area of the visibility (from which the slow decaying trace is subtracted) as a function of the cavity-emitter detuning. For the points corresponding to the detunings −9, 0, and 9 meV, the leftover fragment is plotted in panels on top and represents the contribution of the PSB to the overall interference visibility.

the QD-cavity emission using a bandpass filter with an approximate bandwidth of 2.5 meV (which only passes the QD emission) and conducted a set of first-order correlation measurements using a Michelson interferometer as we change the emitter-cavity detuning [Figs. 3(a) and 3(b)]. Scanning the relative phase between the arms of the interferometer, we obtain interferograms displaying intensity oscillations. Yielding the value of the first-order correlation function for a given temporal delay in the interferometer, the interference visibility v of these oscillations is extracted as $v = (I_{\max} - I_{\min})/(I_{\max} + I_{\min})$, where $I_{\max,\min}$ is, respectively, the upper and lower envelope of the interferogram signal.

In Fig. 3(a), we plot the resulting extracted interference visibility as we coarsely scan our interferometer. The measurements reveal a significant influence of the emitter-cavity detuning on the first-order coherence of the system. While all visibility traces decay with constant coherence time at longer timescales, at very short timescales, the interference visibilities for negative detunings are reduced and deviate from the simple exponential decay. This phenomenon is further investigated in Fig. 3(b) with finer time resolution while showing the visibility in the vicinity of the zero path difference between the two interferometer arms.

The visibility plots exhibit a pronounced fast decay due to the PSB (which approximately is of Gaussian shape, yielding the correct quadratic behavior at small times) and the slowly decaying background that we attribute to the ZPL emission [40,41]. It is in agreement with a recent report on the coherence of a similar WSe_2-based QD [50]. Crucially, the impact of the pronounced fast decay clearly depends on the QD-cavity detuning, whereas the slow decay remains widely unaffected.

Since the interferograms display the temporal coherence profile of the emission, they are connected to the spectral shape of the emission via Fourier transformation (FT). Hence, we can harness the power of our fully microscopic model for the QD-phonon system and express the theoretically obtained visibilities of photon coherence as

$$v(t) = N\left|\int_{-\infty}^{\infty} d\omega I(\omega)H(\omega)e^{i\omega t}\right|. \tag{5}$$

For the emission spectrum $I(\omega)$, we directly use the fit functions shown in Fig. 2(a). The function $H(\omega)$ models a bandpass filter, and N is a normalization constant; for details see the Supplemental Material [36]. To adjust $H(\omega)$ and N, we simultaneously fit the experimental visibility for several detunings [except for the −9.15 meV, for the same reason as for Fig. 2(a)] with the same bandpass parameters. We assume that the deviation of detunings used for interferometry and for spectroscopy are negligible.

Numerical fits to the experimental visibility data using Eq. (5) are shown in Fig. 3(c), where the cavity detuning is varied according to the theoretical spectra shown in Fig. 2(a). We find an overall good agreement with the experimentally obtained temporal coherence, which corroborates the consistency of our microscopic model. The most notable feature that cannot be extracted directly from the experimental data is the pronounced oscillation of the signal at negative detuning with a period of about 1 ps. We attribute it to an interference between the emitter and the cavity-enhanced PSB.

To extend our quantitative analysis and extract coherence times, we fit the experimental data with a more phenomenological model based on the FT of a typical emission

spectrum of such QDs. We approximate the intensity of the signal recorded in the Michelson interferometer as

$$I(t) = I_0 + \frac{A_1}{\tau_1} e^{-\frac{|t|}{\tau_1}} \cos(\omega_1 t) + \frac{A_2}{\tau_2} e^{-\frac{t^2}{\tau_2^2}} \cos(\omega_2 t), \quad (6)$$

where t is the delay between the two arms of the interferometer, I_0 is the intensity of the signal at the input of the interferometer, and $A_{1,2}$, $\tau_{1,2}$, $\omega_{1,2}$ are the amplitudes, decay times, and the frequencies of the individual components, respectively. The extraction of the envelopes is possible by considering the interference of two plane waves, resulting in

$$I_{\max,\min}(t) = I_0 \pm \left\{ \frac{A_1^2}{\tau_1^2} e^{-2\frac{|t|}{\tau_1}} + \frac{A_2^2}{\tau_2^2} e^{-2\frac{t^2}{\tau_2^2}} + 2A_1 A_2 e^{-\frac{|t|}{\tau_1}} e^{-\frac{t^2}{\tau_2^2}} \times \cos(|\omega_1 - \omega_2| t) \right\}^{\frac{1}{2}}. \quad (7)$$

Since the upper and the lower envelopes are symmetric according to Eq. (7), the visibility trace is expressed as $v \propto |I_{\max}|$.

In Fig. 3(a), we perform fitting of the visibility using the function proposed in Eq. (7) without the Gaussian decay term and excluding the range of $[-10, 10]$ ps (shown as shaded area), since the double exponential term is dominant at longer timescales. Our fitting procedure reveals a coherence time associated with the ZPL of 11.8 ± 0.4 ps, which is consistent with the spectral ZPL linewidth of 110 μeV. The value of the coherence time is 2 orders of magnitude smaller than the characteristic radiative lifetime; see the data presented in the Supplemental Material [36].

In Fig. 3(b), the data are fitted with a function proportional to Eq. (7) with τ_1 fixed to 11.8 ps. From the fits for negative detunings, we extract an average fast component $\tau_2 = 0.85 \pm 0.15$ ps, which we adopt as a fixed value for the zero and positive detuning fits.

The described procedure allows us to quantify the PSB contribution to the visibility decay as a function of cavity-emitter detuning. This contribution is most straightforwardly reflected by its relative area below the visibility traces. We extract this area by subtracting the slow decaying (ZPL) trace to obtain the leftover fragments in the top panel of Fig. 3(d). As shown in the bottom panel, the area suggests that the phonon impact on the first-order temporal coherence is of great significance for negative as well as zero detuning conditions, but can be considerably suppressed for positive detunings.

In summary, we provide a novel pathway to cavity of control the optical properties of quantum emitters in general, and WSe_2 QDs in particular. While previous works specifically utilized the coupling of QDs to optical cavities to enhance the photon flux, as well as to engineer the spontaneous emission lifetime, here, we verify that the cavity-emitter detuning directly influences the emitter coherence time (T_2). This significant effect is prominently exposed in the spectral as well in the temporal domain. The way to gain control of the emitter coherence utilizes selective enhancement of the emission of the zero-phonon line versus the rapidly dephasing phonon sideband (which is unavoidable and material specific). Indeed, this method does not require high-Q cavities and works particularly well in the case of WSe_2 QDs featuring a very asymmetric PSB. Our QDs still suffer from a rapidly dephased ZPL that sets limits to the overall temporal coherence. We attribute this effect to the effective dephasing provided by the emitter-phonon interaction in a truly two-dimensional system. Our methodology to engineer the impact of the phonon collisions on the coherence of the emitted light beam is universal and highly relevant in the context of realizing quantum emitters in 2D systems. It will be possible to apply it to the next-generation WSe_2 QDs with reduced dephasing, possibly based on optimized crystals with advanced charge control as well as excited using resonant driving schemes, which will pave the way toward coherent TMDC single-photon sources.

This project was funded within the QuantERA II programme that has received funding from the European Union's Horizon 2020 research and innovation programme under Grant Agreement No. 101017733, and with funding organization the German Federal Ministry of Education and Research (BMBF) within the projects EQUAISE and TubLan Q.0. S. T. acknowledges primary support from NSF Grant No. DMR 2111812 for materials development, NSF Grant No. GOALI 2129412 for scaling, and NSF Grant No. ECCS 2111812 fabrication. C. G. acknowledges funding from the Deutsche Forschungsgemeinschaft priority Program No. SPP2244. We acknowledge partial support from Grant No. DOE-SC0020653 (materials texture development), NSF Grant No. ECCS 2052527 for electronic, and NSF Grant No. DMR 2206987 for magnetic purity tests. C. A.-S. acknowledges the support from the Comunidad de Madrid fund "Atracción de Talento, Mod. 1," ref.2020T1/IND-19785, the project from the Ministerio de Ciencia e Innovación PID2020-113445GB-I00, the project ULTRABRIGHT from the Fundación Ramón Areces, the Grant "Leonardo for researchers in Physics 2023" from Fundación BBVA, and the Comunidad de Madrid and the Spanish State through the Recovery, Transformation, and Resilience Plan ("MATERIALES DISRUPTIVOS BIDIMENSIONALES (2D)" (MAD2D-CM-UAM7), and the European Union through the Next Generation EU funds. M. F. acknowledges support by the Alexander von Humboldt Foundation. A. P. acknowledges the Helene Lange Visiting Professorship program. M. E. acknowledges funding from the University of Oldenburg through a Carl von Ossietzky Young Researchers' Fellowship. Financial support by the

Niedersächsisches Ministerium für Wissenschaft and Kultur within the collaborative project DyNano is acknowledged. C. S. acknowledges the support by the German Research Foundation (Grant No. INST184/220-1 FUGG). A. P. would like to acknowledge the Swedish Research Council (Grant No. 2021-04494).

*Corresponding author: victor.mitryakhin@uni-oldenburg.de

[1] E. Stock, M.-R. Dachner, T. Warming, A. Schliwa, A. Lochmann, A. Hoffmann, A. I. Toropov, A. K. Bakarov, I. A. Derebezov, M. Richter, V. A. Haisler, A. Knorr, and D. Bimberg, Acoustic and optical phonon scattering in a single In(Ga)As quantum dot, Phys. Rev. B **83**, 041304(R) (2011).

[2] C. Galland, A. Högele, H. E. Türeci, and A. Imamoğlu, Non-Markovian decoherence of localized nanotube excitons by acoustic phonons, Phys. Rev. Lett. **101**, 067402 (2008).

[3] T. Grange, N. Somaschi, C. Antón, L. De Santis, G. Coppola, V. Giesz, A. Lemaître, I. Sagnes, A. Auffèves, and P. Senellart, Reducing phonon-induced decoherence in solid-state single-photon sources with cavity quantum electrodynamics, Phys. Rev. Lett. **118**, 253602 (2017).

[4] S. Barzanjeh, A. Xuereb, S. Groeblacher, M. Paternostro, C. A. Regal, and E. M. Weig, Optomechanics for quantum technologies, Nat. Phys. **18**, 15 (2022).

[5] M. Aspelmeyer, T. J. Kippenberg, and F. Marquardt, Cavity optomechanics, Rev. Mod. Phys. **86**, 1391 (2014).

[6] Y. Chu, P. Kharel, T. Yoon, L. Frunzio, P. T. Rakich, and R. J. Schoelkopf, Creation and control of multi-phonon Fock states in a bulk acoustic-wave resonator, Nature (London) **563**, 666 (2018).

[7] J. Kettler, N. Vaish, L. M. de Lepinay, B. Besga, P.-L. de Assis, O. Bourgeois, A. Auffeves, M. Richard, J. Claudon, J.-M. Gerard, B. Pigeau, O. Arcizet, P. Verlot, and J.-P. Poizat, Inducing micromechanical motion by optical excitation of a single quantum dot, Nat. Nanotechnol. **16**, 283 (2021).

[8] M. Weiß, D. Wigger, M. Nägele, K. Müller, J. J. Finley, T. Kuhn, P. Machnikowski, and H. J. Krenner, Optomechanical wave mixing by a single quantum dot, Optica **8**, 291 (2021).

[9] J.-M. Pirkkalainen, S. U. Cho, F. Massel, J. Tuorila, T. T. Heikkilae, P. J. Hakonen, and M. A. Sillanpaeae, Cavity optomechanics mediated by a quantum two-level system, Nat. Commun. **6**, 6981 (2015).

[10] M. Montinaro, G. Wuest, M. Munsch, Y. Fontana, E. Russo-Averchi, M. Heiss, A. Fontcuberta i Morral, R. J. Warburton, and M. Poggio, Quantum dot opto-mechanics in a fully self-assembled nanowire, Nano Lett. **14**, 4454 (2014).

[11] C. hua Liu, J. Zheng, Y. Chen, T. Fryett, and A. Majumdar, Van der waals materials integrated nanophotonic devices (invited), Opt. Mater. Express **9**, 384 (2019).

[12] Y.-M. He, G. Clark, J. R. Schaibley, Y. He, M.-C. Chen, Y.-J. Wei, X. Ding, Q. Zhang, W. Yao, X. Xu, C.-Y. Lu, and J.-W. Pan, Single quantum emitters in monolayer semiconductors, Nat. Nanotechnol. **10**, 497 (2015).

[13] A. Branny, S. Kumar, R. Proux, and B. D. Gerardot, Deterministic strain-induced arrays of quantum emitters in a two-dimensional semiconductor, Nat. Commun. **8**, 15053 (2017).

[14] M. Koperski, K. Nogajewski, A. Arora, V. Cherkez, P. Mallet, J.-Y. Veuillen, J. Marcus, P. Kossacki, and M. Potemski, Single photon emitters in exfoliated WSe_2 structures, Nat. Nanotechnol. **10**, 503 (2015).

[15] C. Chakraborty, L. Kinnischtzke, K. M. Goodfellow, R. Beams, and A. N. Vamivakas, Voltage-controlled quantum light from an atomically thin semiconductor, Nat. Nanotechnol. **10**, 507 (2015).

[16] A. Srivastava, M. Sidler, A. V. Allain, D. S. Lembke, A. Kis, and A. Imamoğlu, Optically active quantum dots in monolayer WSe_2, Nat. Nanotechnol. **10**, 491 (2015).

[17] P. Tonndorf, R. Schmidt, R. Schneider, J. Kern, M. Buscema, G. A. Steele, A. Castellanos-Gomez, H. S. J. v. d. Zant, S. M. d. Vasconcellos, and R. Bratschitsch, Single-photon emission from localized excitons in an atomically thin semiconductor, Optica **2**, 347 (2015).

[18] O. Iff, D. Tedeschi, J. Martín-Sánchez, M. Moczała-Dusanowska, S. Tongay, K. Yumigeta, J. Taboada-Gutiérrez, M. Savaresi, A. Rastelli, P. Alonso-González, S. Höfling, R. Trotta, and C. Schneider, Strain-tunable single photon sources in WSe_2 Monolayers, Nano Lett. **19**, 6931 (2019).

[19] M. Turunen, M. Brotons-Gisbert, Y. Dai, Y. Wang, E. Scerri, C. Bonato, K. Jöns, Z. Sun, and B. Gerardot, Quantum photonics with layered 2D materials, Nat. Rev. Phys. **4**, 219 (2022).

[20] A. Castellanos-Gomez, M. Buscema, R. Molenaar, V. Singh, L. Janssen, H. S. J. van der Zant, and G. A. Steele, Deterministic transfer of two-dimensional materials by all-dry viscoelastic stamping, 2D Mater. **1**, 011002 (2014).

[21] O. Iff, Q. Buchinger, M. Moczała-Dusanowska, M. Kamp, S. Betzold, M. Davanco, K. Srinivasan, S. Tongay, C. Antón-Solanas, S. Höfling, and C. Schneider, Purcell-enhanced single photon source based on a deterministically placed WSe_2 monolayer quantum dot in a circular Bragg grating cavity, Nano Lett. **21**, 4715 (2021).

[22] L. N. Tripathi, O. Iff, S. Betzold, L. Dusanowski, M. Emmerling, K. Moon, Y. J. Lee, S.-H. Kwon, S. Höfling, and C. Schneider, Spontaneous emission enhancement in strain-induced WSe_2 monolayer-based quantum light sources on metallic surfaces, ACS Photonics **5**, 1919 (2018).

[23] T. Cai, J.-H. Kim, Z. Yang, S. Dutta, S. Aghaeimeibodi, and E. Waks, Radiative Enhancement of single quantum emitters in WSe_2 monolayers using site-controlled metallic nanopillars, ACS Photonics **5**, 3466 (2018).

[24] Y. Luo, G. D. Shepard, J. V. Ardelean, D. A. Rhodes, B. Kim, K. Barmak, J. C. Hone, and S. Strauf, Deterministic coupling of site-controlled quantum emitters in monolayer WSe_2 to plasmonic nanocavities, Nat. Nanotechnol. **13**, 1137 (2018).

[25] J.-C. Drawer, V. N. Mitryakhin, H. Shan, S. Stephan, M. Gittinger, L. Lackner, B. Han, G. Leibeling, F. Eilenberger, R. Banerjee, S. Tongay, K. Watanabe, T. Taniguchi, C. Lienau, M. Silies, C. Anton-Solanas, M. Esmann, and C. Schneider, Monolayer-based single-photon source in a liquid-helium-free open cavity featuring 65% brightness and quantum coherence, Nano Lett. **23**, 8683 (2023).

[26] V. Narayanamurti, H. L. Störmer, M. A. Chin, A. C. Gossard, and W. Wiegmann, Selective transmission of high-frequency phonons by a superlattice: The "dielectric" phonon filter, Phys. Rev. Lett. **43**, 2012 (1979).
[27] M. Trigo, A. Bruchhausen, A. Fainstein, B. Jusserand, and V. Thierry-Mieg, Confinement of acoustical vibrations in a semiconductor planar phonon cavity, Phys. Rev. Lett. **89**, 227402 (2002).
[28] O. Florez, G. Arregui, M. Albrechtsen, R. C. Ng, J. Gomis-Bresco, S. Stobbe, C. M. Sotomayor-Torres, and P. D. García, Engineering nanoscale hypersonic phonon transport, Nature Nanotech. **17**, 947 (2022).
[29] M. Esmann, F. R. Lamberti, A. Harouri *et al.*, Brillouin scattering in hybrid optophononic Bragg micropillar resonators at 300 GHz, Optica **7**, 854 (2019).
[30] B. Jusserand and M. Cardona, Raman spectroscopy of vibrations in superlattices, in *Light Scattering in Solids V: Superlattices and Other Microstructures*, edited by M. Cardona and G. Güntherodt (Springer, Berlin, 1989), pp. 49–152.
[31] M. Cazayous, J. Groenen, J. R. Huntzinger, A. Mlayah, and O. G. Schmidt, Spatial correlations and Raman scattering interferences in self-assembled quantum dot multilayers, Phys. Rev. B **64**, 033306 (2001).
[32] B. Spokoyny, H. Utzat, H. Moon, G. Grosso, D. Englund, and M. G. Bawendi, Effect of spectral diffusion on the coherence properties of a single quantum emitter in hexagonal boron nitride, J. Phys. Chem. Lett. **11**, 1330 (2020).
[33] S. White, C. Stewart, A. S. Solntsev, C. Li, M. Toth, M. Kianinia, and I. Aharonovich, Phonon dephasing and spectral diffusion of quantum emitters in hexagonal boron nitride, Optica **8**, 1153 (2021).
[34] M. Brotons-Gisbert, A. Branny, S. Kumar, R. Picard, R. Proux, M. Gray, K. S. Burch, K. Watanabe, T. Taniguchi, and B. D. Gerardot, Coulomb blockade in an atomically thin quantum dot coupled to a tunable Fermi reservoir, Nat. Nanotechnol. **14**, 442 (2019).
[35] Z.-W. Wang, Y. Xiao, J.-P. Deng, Y. Cui, and Z.-Q. Li, Multiphonon Raman scattering mediated by the exciton states in monolayer transition metal chalcogenides, Phys. Rev. B **100**, 125308 (2019).
[36] See Supplemental Material at http://link.aps.org/supplemental/10.1103/PhysRevLett.132.206903 for more details about the sample, additional experimental data, and the full description of the fitting procedure based on the independent boson model. Supplemental Material includes Refs. [20,25,37–48]).
[37] C. B. Duke and G. D. Mahan, Phonon-broadened impurity spectra. I. Density of states, Phys. Rev. **139**, A1965 (1965).
[38] J. Klein, M. Lorke, M. Florian, F. Sigger, L. Sigl, S. Rey, J. Wierzbowski, J. Cerne, K. Mueller, E. Mitterreiter, P. Zimmermann, T. Taniguchi, K. Watanabe, U. Wurstbauer, M. Kaniber, M. Knap, R. Schmidt, J. J. Finley, and A. W. Holleitner, Site-selectively generated photon emitters in monolayer MoS_2 via local helium ion irradiation, Nat. Commun. **10**, 2755 (2019).
[39] D. Wigger, R. Schmidt, O. D. Pozo-Zamudio, J. A. Preuss, P. Tonndorf, R. Schneider, P. Steeger, J. Kern, Y. Khodaei, J. Sperling, S. M. de Vasconcellos, R. Bratschitsch, and T. Kuhn, Phonon-assisted emission and absorption of individual color centers in hexagonal boron nitride, 2D Mater. **6**, 035006 (2019).
[40] B. Krummheuer, V. M. Axt, and T. Kuhn, Theory of pure dephasing and the resulting absorption line shape in semiconductor quantum dots, Phys. Rev. B **65**, 195313 (2002).
[41] R. Zimmermann and E. Runge, Dephasing in quantum dots via electron-phonon interaction, *Proceedings of the 26th ICPS, Edinburgh* (2002).
[42] G. D. Mahan, *Many-Particle Physics* (Plenum Press, New York, 1993).
[43] P. Kaer, P. Lodahl, A.-P. Jauho, and J. Mork, Microscopic theory of indistinguishable single-photon emission from a quantum dot coupled to a cavity: The role of non-Markovian phonon-induced decoherence, Phys. Rev. B **87**, 081308(R) (2013).
[44] J. Ye, Y. Zhao, N. Ng, and J. Cao, Width of phonon sidebands in the Brownian oscillator model, J. Phys. Chem. B **113**, 5897 (2009).
[45] M. Kira, F. Jahnke, W. Hoyer, and S. W. Koch, Quantum theory of spontaneous emission and coherent effects in semiconductor microstructures, Prog. Quantum Electron. **23**, 189 (1999).
[46] C. N. Böttge, T. Feldtmann, M. Kira, and S. W. Koch, Phonon sidebands in the semiconductor microcavity luminescence, Phys. Status Solidi (c) **8**, 1220 (2011).
[47] A. Azzalini, A class of distributions which includes the normal ones, Scand. J. Stat. Theory Appl. **12**, 171 (1985), https://www.jstor.org/stable/4615982.
[48] M. Newville, T. Stensitzki, D. B. Allen, and A. Ingargiola, LMFIT: Non-linear least-square minimization and curve-fitting for PYTHON, 10.5281/zenodo.11813.
[49] E. M. Purcell, Spontaneous emission probabilities at radio frequencies, in *Confined Electrons and Photons: New Physics and Applications*, edited by E. Burstein and C. Weisbuch (Springer, Boston, 1995), pp. 839–839.
[50] M. von Helversen, L. Greten, I. Limame, C.-W. Shih, P. Schlaugat, C. Antón-Solanas, C. Schneider, B. Rosa, A. Knorr, and S. Reitzenstein, Temperature dependent temporal coherence of metallic-nanoparticle-induced single-photon emitters in a WSe_2 monolayer, 2D Mater. **10**, 045034 (2023).